Influence of the Base Element on the Thermal Properties of Non- Ferrous Chromium-Rich TaC-Containing Alloys Elaborated by Conventional Casting: Part 2: Thermogravimetric and Metallographic Study of the Oxidation Start and of the Oxide Scale Spallation

Patrice Berthod, Lionel Aranda, Ghouti Medjahdi, Jean-Paul K Gomis

Influence of the Base Element on the Thermal Properties of Non-Ferrous Chromium-Rich TaC-Containing Alloys Elaborated by Conventional Casting: Part 2: Thermogravimetric and Metallographic Study of the Oxidation Start and of the Oxide Scale Spallation

Patrice Berthod[1,*], Lionel Aranda[1], Ghouti Medjahdi[1] and Jean-Paul K. Gomis[2]

[1]*Institut Jean Lamour (UMR 7198), University of Lorraine, Campus ARTEM, 2 allée André Guinier, BP 50840, 54000 Nancy, France*

[2]*Faculty of Science and Technologies, Campus Victor Grignard, Rue du Jardin Botanique, BP 70239 54500 Vandoeuvre-lès-Nancy, France*

Abstract: After a first part devoted to the study of several thermal chemical and mechanical characteristics of the six (xCo-yNi, bal.)-25Cr-0.4C-6Ta alloys, this second part of their study deals with the oxidation behaviour of these alloys in presence of heating or of cooling. The heating and cooling parts of thermogravimetry files of oxidation tests of which the isothermal parts were earlier studied, were analysed by plotting mass variation versus temperature. During heating the oxidation starts and a first mass gain is achieved prior to the isothermal stage. They are slightly influenced by the Co/Ni ratio. During the cooling oxide scale spallation happens for all alloys. For the nickel-richest alloys this phenomenon takes place for a temperature less decreased in comparison to the cobalt-based alloys. The fall in mass due to the loss of oxides by spallation seems a little higher for the nickel-richest alloys than that for the cobalt-richest ones. More than to differences in thermal expansion coefficient, this difference may be linked to the oxidation-induced mass gain achieved prior to spallation start, which is higher for the cobalt-richest alloys than for the nickel-richest ones.

Keywords: Cast alloys for high temperature, nickel and cobalt, tantalum carbides, thermogravimetry, oxidation start, oxide scale spallation.

INTRODUCTION

Tantalum is present in the chemical compositions of many cast superalloys [1]. Due to its strong carbide-former behaviour and its atomic size and weight, it may be very useful for creep resistance by obstructing the dislocations movement and the interdendritic debonding. For instance one can meet about 1wt.%Ta in the B1900+Hf Ni-based superalloy [2] or up to 2wt.%Ta in the IN617 one [3]. Classical cobalt-based alloys may also contain tantalum for the same purpose [4] but this is also true for new generation Co-based alloys such as the emerging Co-Re family [5]. Higher Ta contents can be found in other superalloys, in Co-based ones for instance [6]. Tantalum is also a highly oxidable element and its oxidation as well as the oxidation of carbon on the alloy surface may induce the destabilization of the TaC carbides which are the closest to the oxidation front. The release in both Ta and C which diffuse towards the oxidation front induces a propagation of the dissolution of TaC and the Ta and C outward diffusion. This effect on the strengthening of the alloy at the subsurface scale, is also accompanied by an accumulation of Ta forming growing oxide very close to the subsurface. These oxides were suspected to be responsible of a lack of adherence of the external oxide scale (mainly of chromia) and its rupture and loss when temperature varies. This was for example observed and interpreted in this way during the cooling of oxidized nickel-chromium alloys in [7]. Such a secondary effect of the presence of tantalum in superalloys is potentially particularly deleterious for the progress of the general deterioration of superalloys during thermal cycling which is a very common situation of work for high temperature service components. For such alloy, a repeated loss of protective external oxide scale, followed by the reformation of a new one, accelerates the impoverishment of the subsurface in chromium. Consequently this also accelerates the final destruction of the alloy by general catastrophic oxidation [8].

The purpose of the present work is the study of the thermal properties of alloys which all contain significant weight contents in tantalum to allow obtaining a TaC interdendritic carbide network to achieve high mechanical resistance at high temperature. Due to this, the same problem of non ideal adherence of the formed oxide scales consequently to the oxidation of

Address correspondence to this article at the Institut Jean Lamour (UMR 7198), University of Lorraine, Campus ARTEM, 2 allée André Guinier, BP 50840, 54000 Nancy, France; Tel: (+33) 3 72 74 27 29;
E-mail: patrice.berthod@univ-lorraine.fr

E-ISSN: 2410-4701/19

Ta at the scale/alloy frontier earlier observed for nickel-chromium alloys [7], may also concern the different Co-added versions of the same nickel–based alloy. Thermogravimetry runs were performed to specifically investigate the scale spallation parameters during cooling, but also to the start of oxidation during heating. Results were analysed according to another method than what is usually done with mass variation measurements in oxidation. The results will be analysed versus the Co content in order to detect any evolution of behaviour by progressively going from nickel-base to cobalt-base.

MATERIALS AND METHODS

Thermogravimetric Runs

Samples were extracted from the same ingots as in the first part of this work [8]. In order to obtain an external surface great enough for an accurate measurement of the mass changes due to oxidation, they were cut with a shape globally triangular imposed by the general outer shape of the ingot. The obtained samples were ground with SiC papers (#1200) on their main faces and edges and corners were smoothed using the same SiC papers. The used thermobalance was a SETARAM TG92 one and tests were carried out under a constant flow of synthetic air ($80\%N_2$-$20\%O_2$). The applied thermal cycle was composed of a heating at +20°C/min from ambient temperature up to 1250°C, an isothermal stage at this temperature during 70 hours and a cooling down to ambient temperature at -5°C/min.

Exploitation of the Oxidation Tests

The mass gain versus time files were first corrected from the air buoyancy variations during the heating and the cooling with a method described in an earlier work [9]. Mass gain was plotted versus temperature, instead versus time as usually done for thermogravimetric results. The obtained curves were analysed in their heating parts and in their cooling part. During the heating, oxidation starts as soon as temperature is high enough but the associated mass gain, too low, is not detectable by the microbalance present in the apparatus. This is only when temperature has become high enough that the mass gain can be detected. This value of temperature at which the mass gain curve starts quitting the abscissa axis is noted. Oxidation and consequently mass gain both accelerates during the following heating until reaching the temperature of the isothermal stage. At this time a small but significant mass gain only achieved during the heating can also be noted. During the 70 hours of isothermal oxidation the main part of mass gain is obtained. The total mass gain achieved at the end of the 70h-long isothermal stage is also noted. During the cooling oxidation slows down because of the decrease in temperature, but the mass gain goes on increasing more and more slowly. After more or less hundreds of Celsius degrees of cooling the curve may suddenly fall (temperature noted) and becomes definitely irregular until return at ambient temperature (final mass variation noted).

Metallographic Observation of the Oxidized Surfaces

The oxidized samples were carefully extracted from the alumina-gained platinum suspension and handled. They were first examined with the naked eye and by low magnification optical observation. Thereafter they were subjected to X-ray diffraction (XRD) using a Bruker D8 Advance diffractometer to identify the oxides remained on surface and confirm the presence of emerging denuded alloy.

RESULTS AND DISCUSSION

Oxidation and Mass Gain during Heating

After {Δm/S versus T}-plotting and air buoyancy variations correction, the temperature of oxidation start during the heating phase was determined for all the six alloys. An enlargement of this part of the {Δm/S versus T} curves is presented in Figure **1** for the two nickel-richest alloys (0Co5NiTa and 1Co4NiTa), in Figure **2** for the two intermediate alloys (2Co3NiTa and 3Co2NiTa) and in Figure **3** for the two cobalt-richest alloys (4Co1NiTa and 5Co0NiTa). One can see on all curves that the oxidation-induced mass gain becomes detectable between 800 and 1000°C and that, after, it clearly accelerates with the increase in temperature. The temperature of oxidation start was noted on all the six curves and the results are plotted in Figure **4** (top), alloy by alloy, as is to say indirectly versus the Co content in alloy.

Obviously no systematic evolution of this temperature of oxidation start detection is evidenced versus the chemical composition of the alloy, even if one can feel in a first time that this temperature tends to decrease when the Co content increases, as is to say that oxidation during heating tends to be more precocious when the Co content increases. Concerning the total mass gain by oxidation achieved during the whole heating, represented in the same Figure **4**

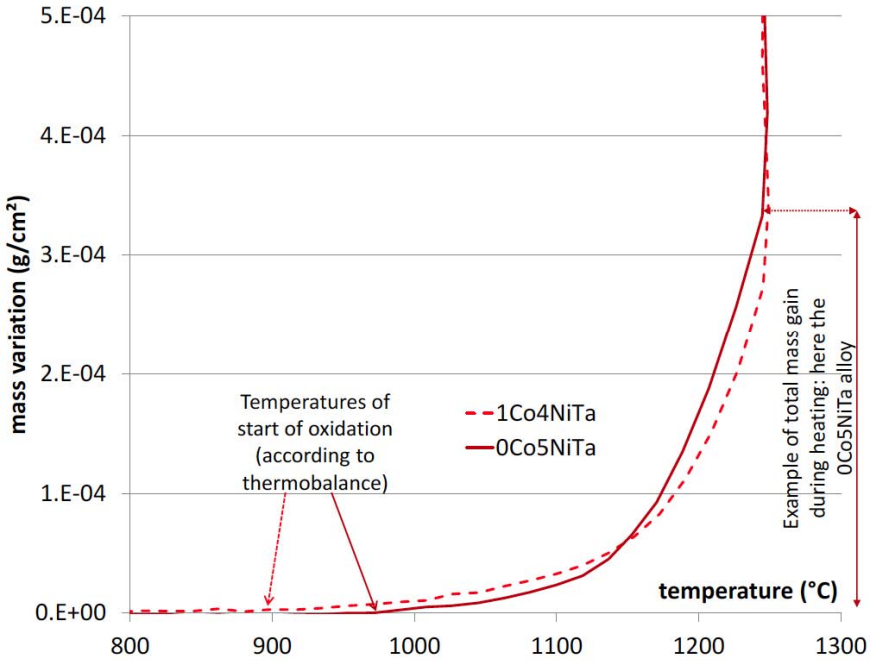

Figure 1: The heating parts of the {Δm/S versus T} curves obtained for the two nickel-richest alloys.

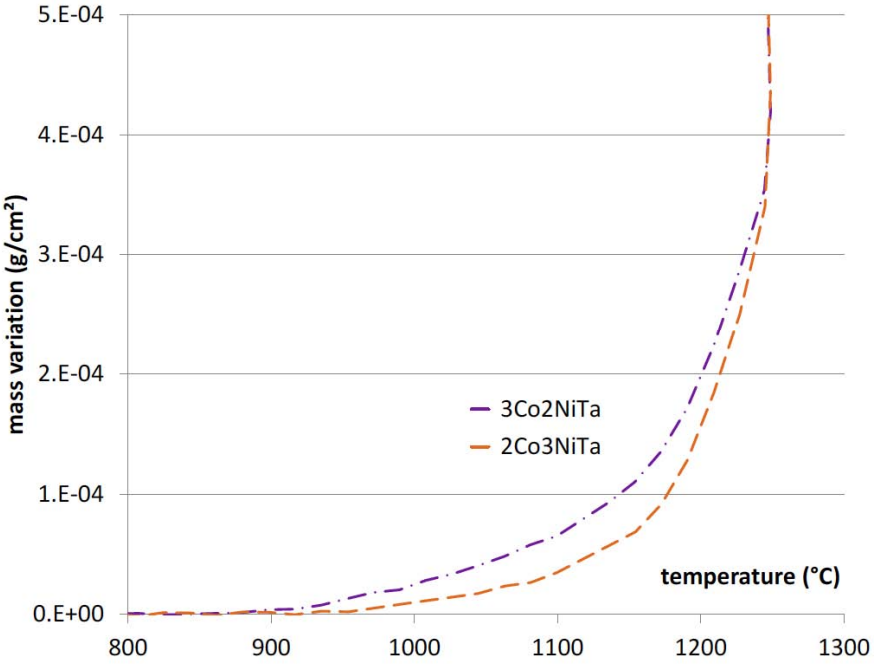

Figure 2: The heating parts of the {Δm/S versus T} curves obtained for the two intermediate alloys.

(bottom), the results are rather scattered despite that, here too, a tendency seems existing: the total mass gain tends to increase when the Co content increases. A more precocious start of oxidation and a greater mass gain achieved at the end of heating appear as being consistent.

In the heating parts of the curves, after the start of oxidation according to the beginning of the detection of the mass gain by the thermobalance, the elementary mass gain divided by the time step, estimation of the linear constant at the current value of temperature, was calculated and its Neperian logarithm was plotted versus the reciprocal absolute temperature. The obtained graphs contained a major part which was linear, this suggesting that the linear constant well obeyed an Arrhenius law. The corresponding activation energies were deduced from the slope of the straight

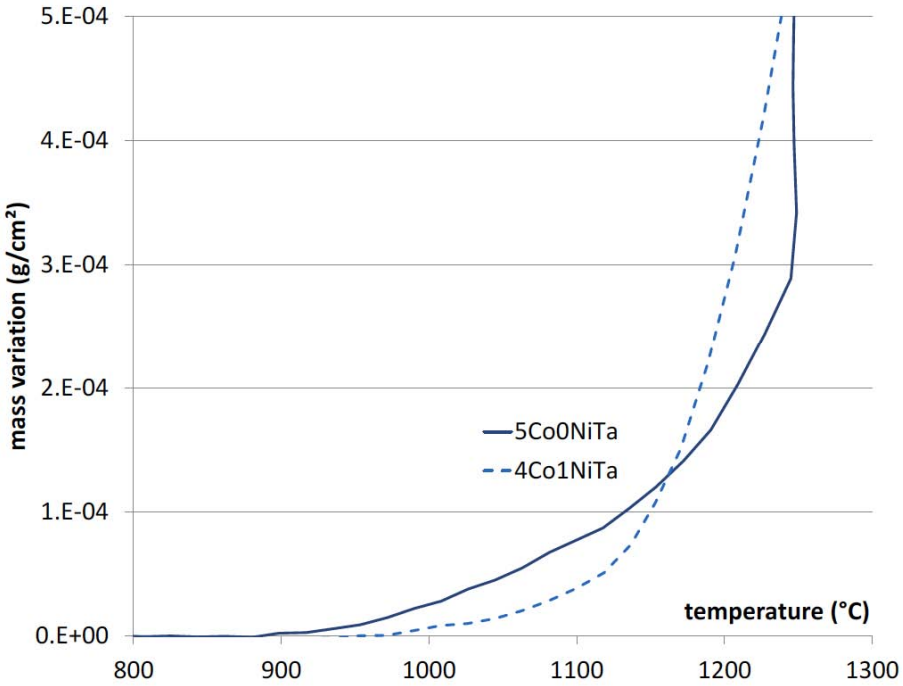

Figure 3: The heating parts of the {Δm/S versus T} curves obtained for the two cobalt-richest alloys.

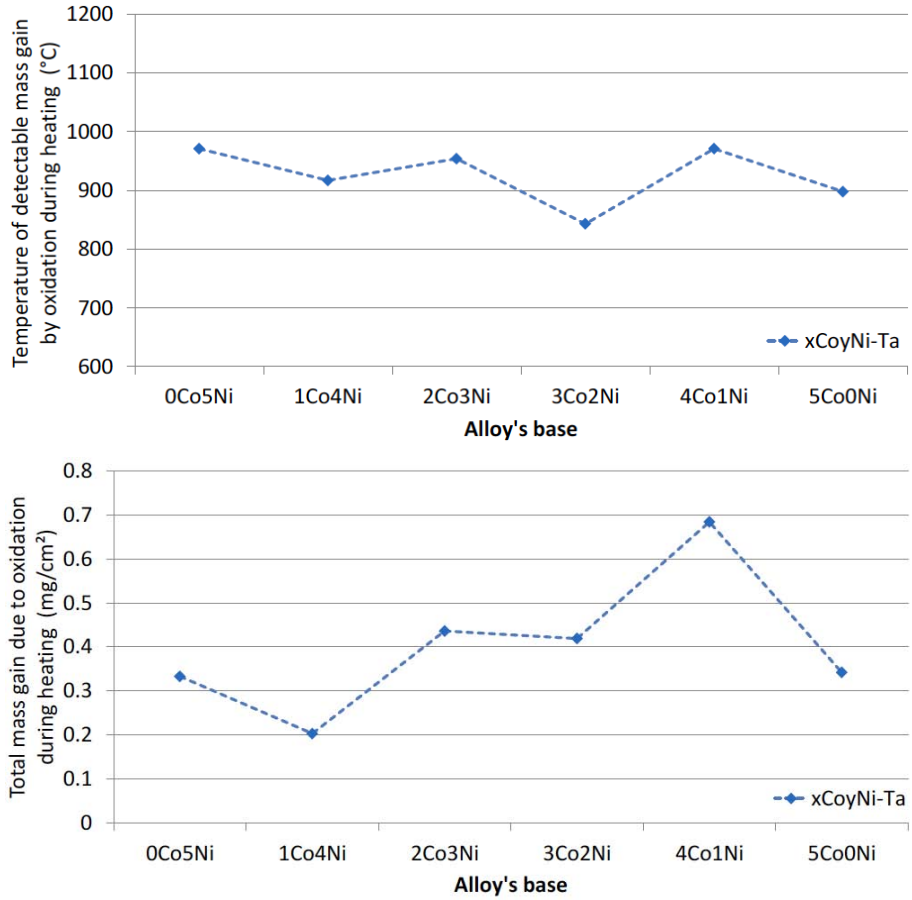

Figure 4: The temperature of oxidation start at heating (top) and the total mass gain achieved by oxidation during the whole heating (bottom), both plotted versus the Co content in alloy.

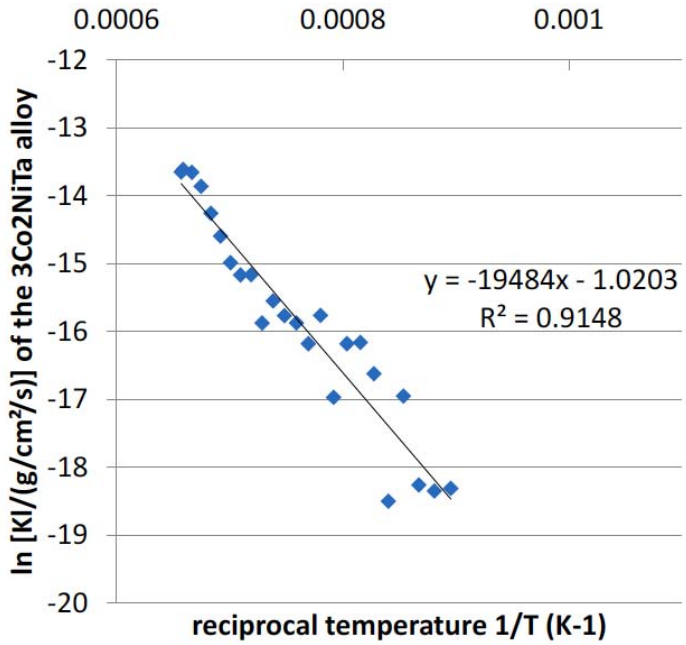

Figure 5: Example of Arrhenian plot of the linear oxidation constant; the corresponding activation energy is calculated by multiplying the -19484 K slope by the opposite value of the perfect gases constant (8.314 J mol^{-1} K^{-1}).

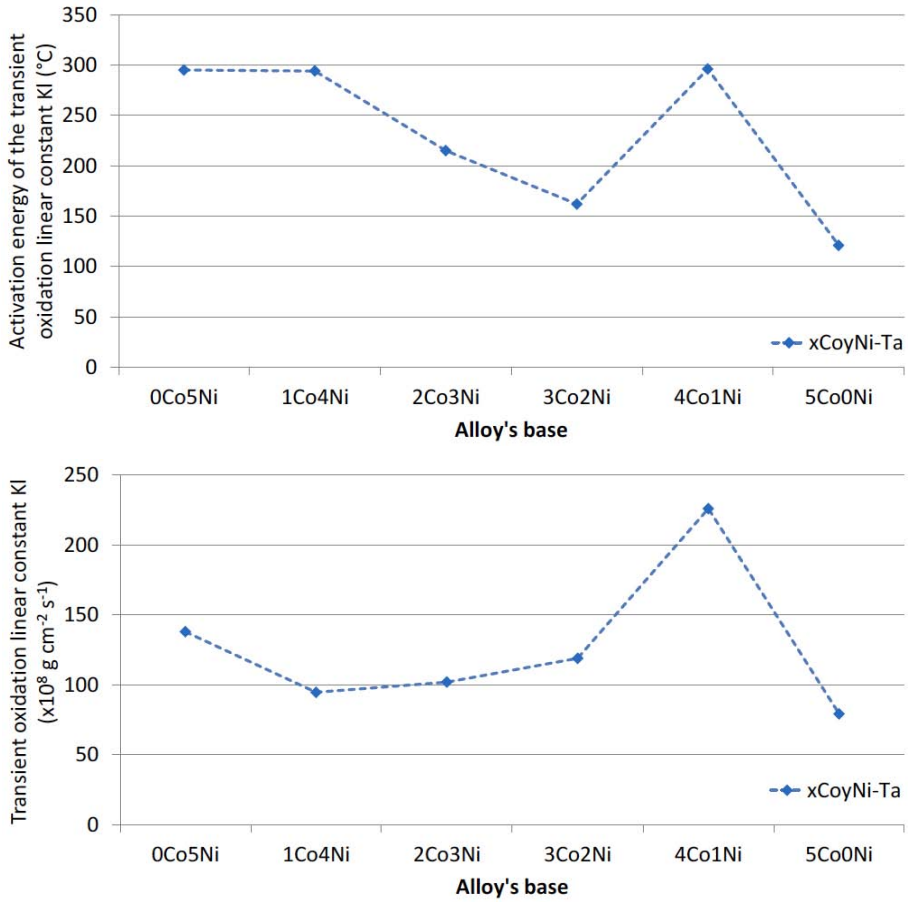

Figure 6: The activation energy stepping in the Arrhenius formula obeyed by the linear constant of instantaneous mass gain rate during heating (top), and the final value of this linear constant when reaching the temperature of the isothermal stage (bottom), both plotted versus the Co content in alloy.

line (example in Figure **5**) and results are plotted in the top part of Figure **6**. The final value of the linear constant, determined as being the slope of the straight line tangent to the classically plotted {Δm/S versus t}-curve, was also noted. These two types of results are graphically given versus the Co content in alloy in the bottom part of Figure **6**. Concerning the activation energies, three of them are close to 300kJ/mol while the three other are lower. No systematic dependence on the chemical composition of the alloy is evident. However, it is possible to imagine a tendency to a decrease in activation energy when the Co content increases but there is a singular point with the 4Co1NiTa alloy. No systematic dependence is visible in the case for the linear oxidation constant at the arrival at the beginning of the isothermal stage; but here too the 4Co1NiTa alloy plays a particular role since the linear constant appears as globally decreasing when the Co content increases if the point corresponding to this alloy is removed.

Oxide Scale Spallation during Cooling

Just after the end of the isothermal stage a cooling programmed with a rate of -5°C/min – rather low rate chosen to try preventing oxide spallation – took place. This was not really successful since, after a 200 to 400°C cooling, the curves became more or less irregular knowing a progressive loss of mass for some of them, and even a sudden fall for the others. The whole {Δm/S versus T} curves are plotted in Figure **7** for the two nickel-richest alloys, in Figure **8** for the two intermediate alloys and in Figure **9** for the two cobalt-richest alloys. Their exploitations led to the results graphically presented in Figures **10** and in **11**. Again, the results corresponding to the 4Co1NiTa alloy in Figures **10** and **11** appear as particular. These new observations concerning this sample, added to the previously presented ones, led to temporarily exclude this alloy. This allows observing much clearly an increase in the total mass gain achieved and a decrease in spallation start temperature when there is more and more cobalt instead nickel in the alloy (Figure **10**). The decrease in spallation start temperature suggests that the resistance of the external oxide scale to spallation becomes better and better when the mass of oxide per surface unit area and thus when the oxide scale thickness increases. At the same time, the total mass of oxide lost during cooling because of spallation tends to be more limited as well as the total mass variation for the whole thermal cycle (Figure **11**).

Surface Metallographic Characterization of the Oxidized Samples

The surface states of the six thermogravimetric samples after oxidation test are shown by optical macrographs (acquired using a Canon Lide 210 office scanner), in the top of Figure **12**. One can easily see the parts of alloys having lost the oxide scales formed

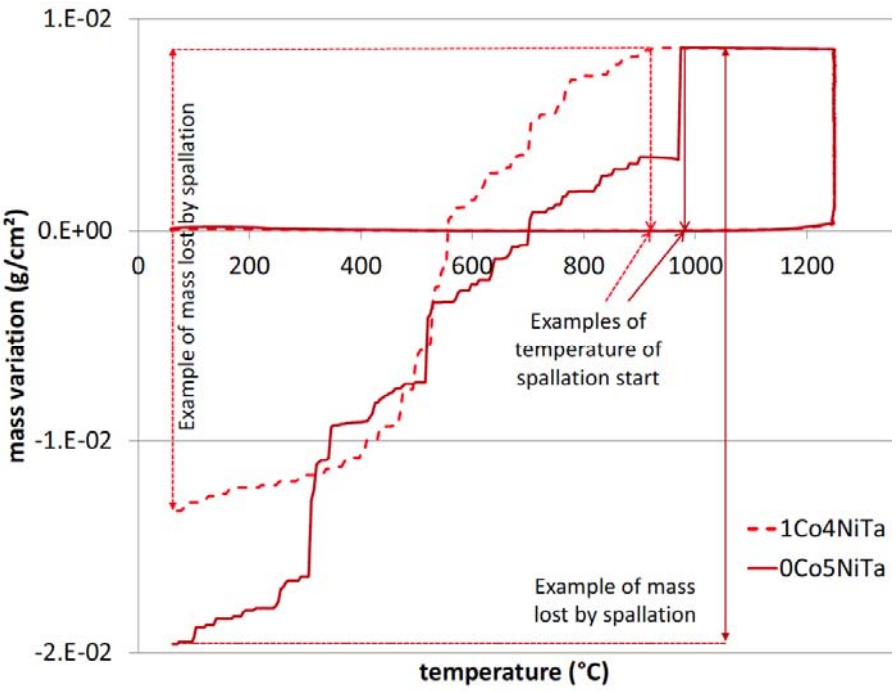

Figure 7: The whole {Δm/S versus T} curves obtained for the two nickel-richest alloys and examples of determination of some parameters characterizing the oxide scale spallation phenomenon.

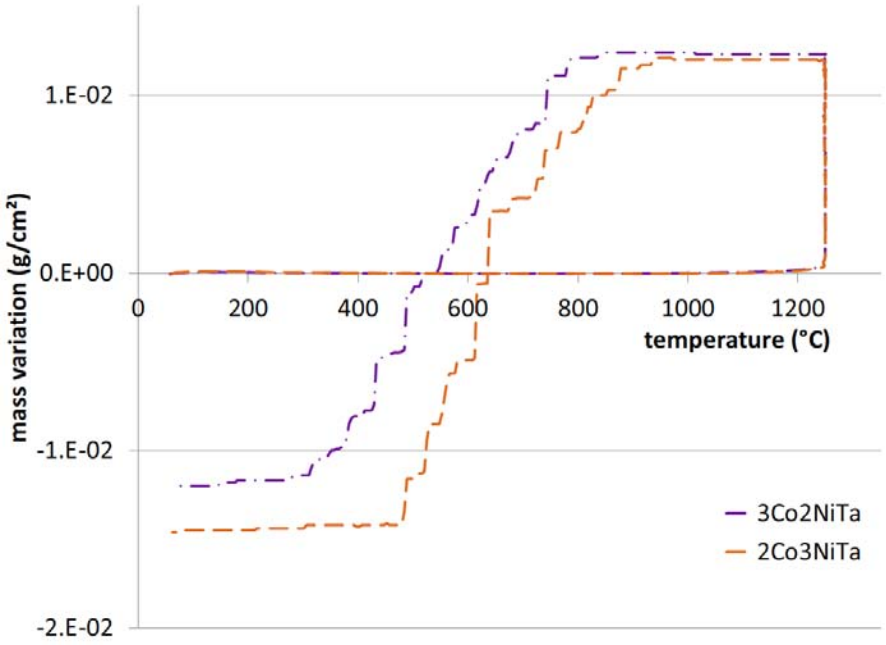

Figure 8: The whole {Δm/S versus T} curves obtained for the two intermediate alloys.

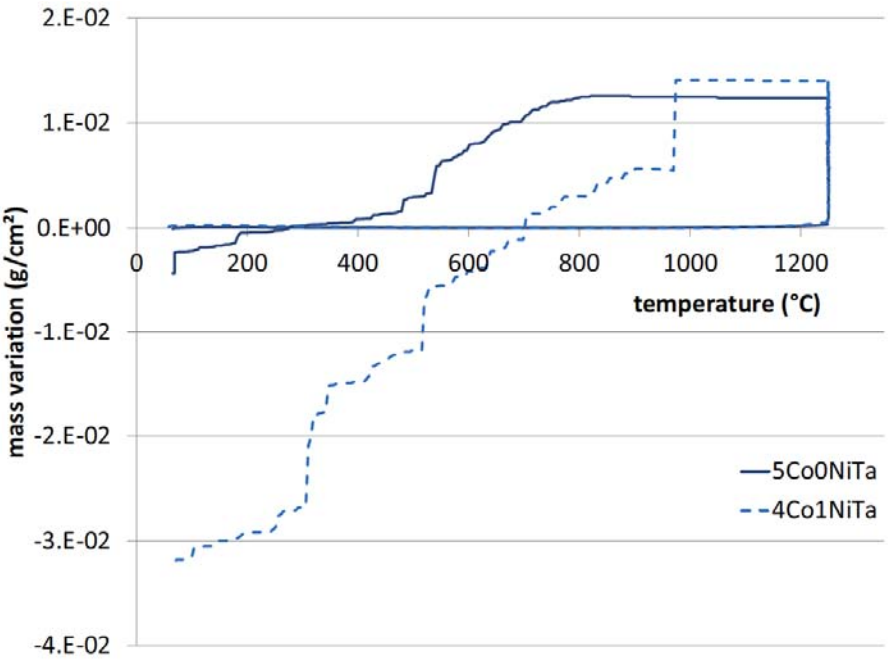

Figure 9: The whole {Δm/S versus T} curves obtained for the two cobalt-richest alloys.

over them during the 70 hours of oxidation at 1250°C. They are clearer than the dark grey remaining oxides. Effectively the nickel-richest alloys suffered more of oxide spallation than the cobalt-richest ones.

In the same Figure **12** two examples of XRD spectra are given, one for a nickel-rich alloy (1Co4NiTa) and one for a cobalt-rich one (4Co1NiTa). In all cases chromia (Cr_2O_3) and the complex oxide of chromium and tantalum ($CrTaO_4$) are present in the remaining part of the external oxide, with additionally the $CoCr_2O_4$ spinel oxide, and even CoO, in the cases of the cobalt-richest alloys. The matrix is also detected by XRD for all the samples but the corresponding diffraction peaks are higher in the case of the nickel-richest alloys than in the case of the cobalt-richest ones, confirming that the first ones have known oxide spallation more than the second ones. Thus good agreement exists between what the cooling parts of the

thermogravimetric curves show and the post-mortem examination of the samples' surfaces.

CONCLUSIONS

Plotting the mass variation results according to the {Δm/S versus T} graphical system allowed observing interesting effects of the Co/Ni balance on first the start of surface oxidation during the heating phase of the thermogravimetric experiments, and second on the sequences of the oxide spallation occurring during the cooling phase following the isothermal stage. Concerning oxidation at heating it is interesting to note that, according to the thermobalance, the cobalt-richest alloys tends to oxidize a little sooner than the nickel-richest ones and that the mass gain achieved at the end of heating tends to be higher. Differences were seen between the activation energies in the Arrhenius

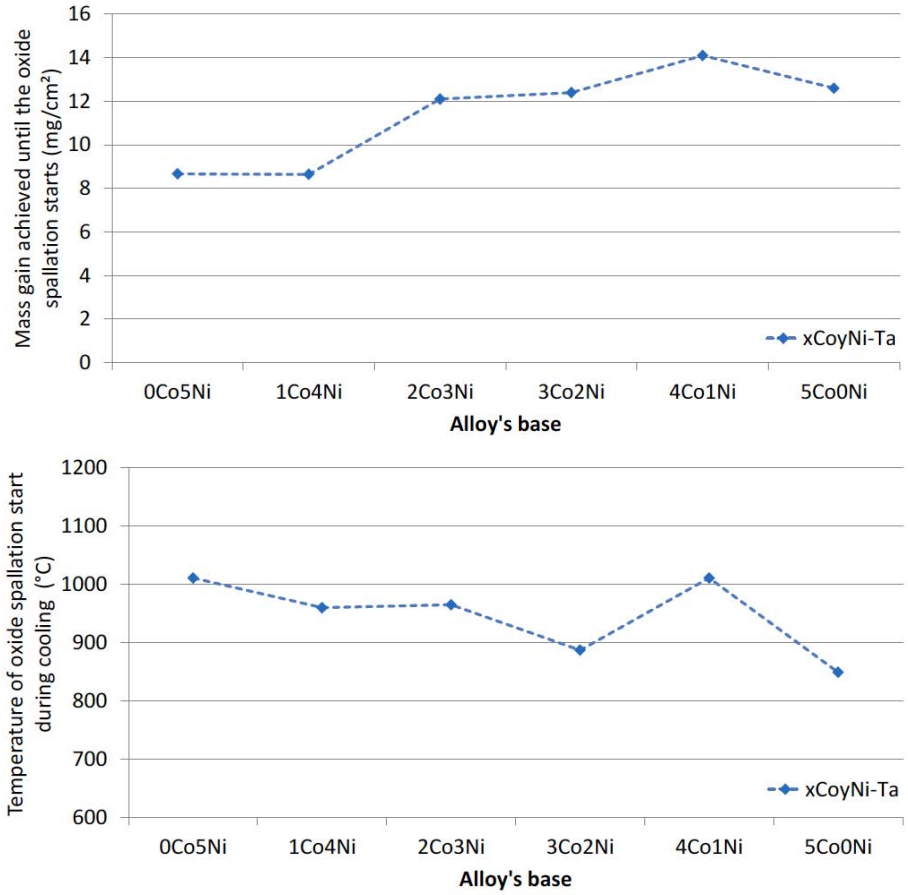

Figure 10: Plot of the total mass gain achieved until spallation starts (top) and of the temperature at which the external oxide starts to spall off during the cooling (bottom).

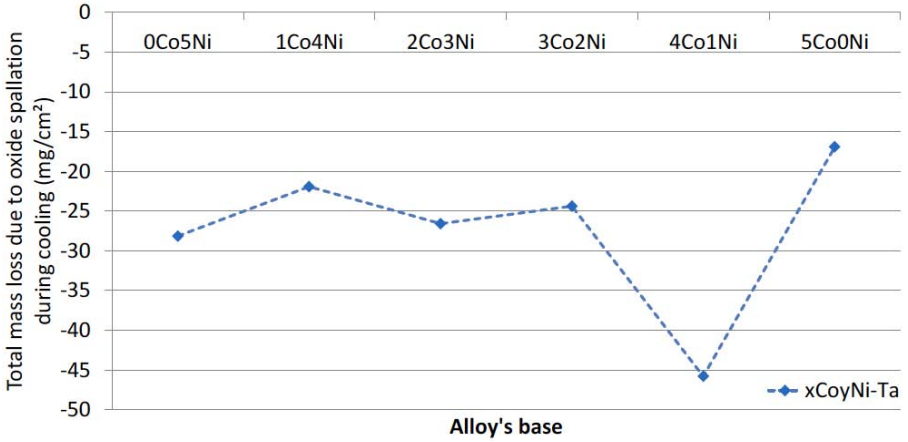

(Figure 11). Continued.

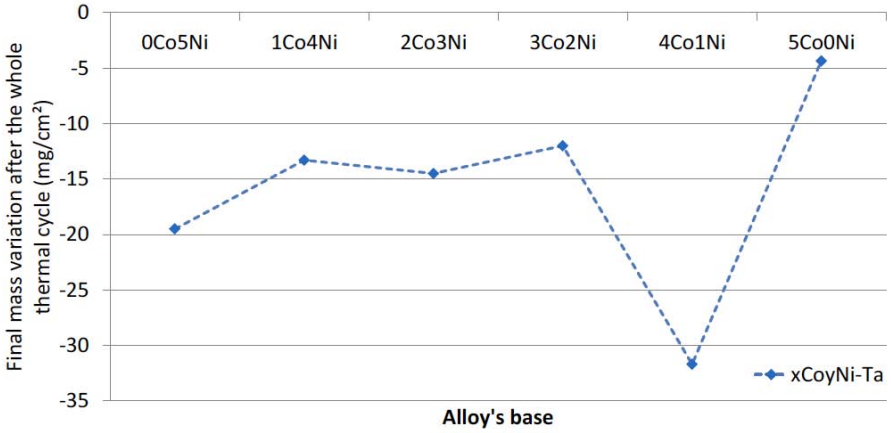

Figure 11: Plot of the total mass lost by surface unit area due to spallation at cooling (top) and of the total mass variation over the whole thermal cycle (bottom).

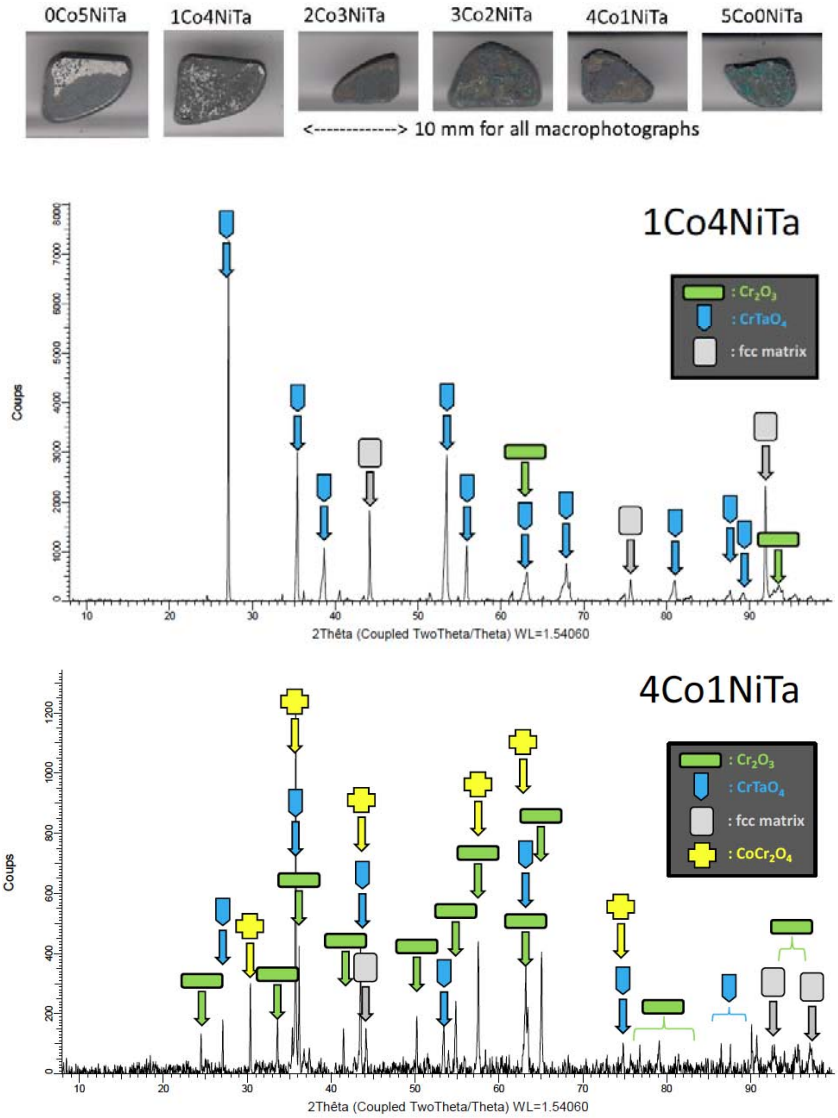

Figure 12: Macrographs showing one of the oxidized main faces of thermogravimetric samples (top) and two examples of obtained XRD patterns allowing the oxides identification (bottom).

laws governing the linear oxidation constant. These differences suggest possible difference in nature of the first oxides to appear. To deepen the investigations for better knowledge of what occurs, additional tests can be envisaged, such as *in situ* XRD follow-up during heating in similar atmosphere (but with lower pressure) with the same heating rate in a diffractometer equipped for allowing such experiment. Concerning oxide spallation during cooling, which happened for all alloys despite the low cooling rate, little differences were detected between the nickel-richest alloys and the cobalt-richest ones: the first ones tended to know oxide spallation a little sooner (i.e. with a lower temperature decrease) than the second ones. Since the average thermal coefficients measured in the first part of this study [8] tended to be lower for the Ni-richest alloys than for the Co-richest ones (i.e. closer to the low values of oxides), it appears that this is possibly due to the thicker external oxide scales of the second alloys by comparison for the first ones, but also to their natures.

The oxidation products, as well as the subsurface oxidation-induced deterioration, will be specifically investigated in the third and final part of this work [10], in order to better understand some of the results obtained in this second part, and also to value the amount of overall degradation in relation with the Co/Ni proportions in these alloys.

REFERENCES

[1] Donachie MJ, Donachie SJ. Superalloys: A Technical Guide (2nd edition), ASM International, Materials Park 2002.

[2] Janowski GM, Harmon BS, Pletka BJ. Metallurgical Transactions A: Physical Metallurgy and Materials Science 1987; 18A(8): 1341. https://doi.org/10.1007/BF02646648

[3] Gao S, Hou J, Yang F, Guo Y, Wang C, Zhou L. Materials Science abd Engineering A: Structural Materials: Properties, Microstructure and Processing 2017; 706: 153. https://doi.org/10.1016/j.msea.2017.09.014

[4] Montazeri M, Ghaini FM, Farnia A. International Journal of Materials Research 2011; 102(12): 1446. https://doi.org/10.3139/146.110616

[5] Gilles R, Mukherji D, Karge L, Strunz P, Beran P, Barbier B, Kriele A, Hofman M, Eckerlebe H, Roesler J. Journal of Applied Crystallography 2016; 49(4): 1253. https://doi.org/10.1107/S1600576716009006

[6] Berthod P, Bernard JL, Liébaut C. Patent, WO2001090429 A1 20011129.

[7] Berthod P, Vébert C, Aranda L. Journal of Materials Science 2007; 42: 352. https://doi.org/10.1007/s10853-006-1033-4

[8] Aranda L, Berthod P, Gomis J-PK, Himeur Z. Journal of Materials Science and Technology Research 2019; 6: 53-62. https://doi.org/10.15377/2410-4701.2019.06.7

[9] Berthod P. The Open Corrosion Journal 2009; 2: 61. https://doi.org/10.2174/1876503300902010061

[10] Gomis J-PK, Berthod P, Etienne E. Journal of Materials Science and Technology Research 2019; 6: 73-83. https://doi.org/10.15377/2410-4701.2019.06.9

Received on 03-10-2019 Accepted on 17-10-2019 Published on 25-10-2019

DOI: https://doi.org/10.15377/2410-4701.2019.06.8